

# The formation of labyrinths, spots and stripe fragments: Applications to cardiovascular calcification and bone regeneration

A Yochelis<sup>1,4</sup>, Y Tintut<sup>1</sup>, L L Demer<sup>1,2</sup> and A Garfinkel<sup>1,3</sup>

<sup>1</sup>Department of Medicine (Cardiology), <sup>2</sup>Department of Physiology, <sup>3</sup>Department of Physiological Science, University of California, Los Angeles, CA 90095

**Abstract.** Calcification and mineralization are fundamental physiological processes, yet the mechanisms of calcification, in trabecular bone and in calcified lesions in atherosclerotic calcification, are unclear. Recently, it was shown in *in vitro* experiments that vascular-derived mesenchymal stem cells can display self-organized calcified patterns. These patterns were attributed to activator/inhibitor dynamics in the style of Turing, with bone morphogenetic protein 2 (BMP-2) acting as an activator, and matrix GLA protein (MGP) acting as an inhibitor. Different pattern morphologies were produced by external application of the inhibitor MGP. Motivated by this qualitative activator-inhibitor dynamics, we study here a bistable form of the Gierer-Meinhardt model, with autocatalytic saturation. Through a detailed analysis in one and two dimensions, we explore the pattern formation mechanisms of steady state patterns, including their dependence on initial conditions. These patterns range from localized holes to labyrinths and localized peaks, or in other words, from dense to sparse activator distributions (respectively). We believe that an understanding of the wide spectrum of activator-inhibitor patterns discussed here is prerequisite to their biochemical control. The mechanisms of pattern formation suggest therapeutic strategies applicable to bone formation in atherosclerotic lesions in arteries (where it is pathological) and to the regeneration of trabecular bone (recapitulating normal physiological development).

## Contents

1. Introduction.....	2
2. Activator-inhibitor model equations .....	2
3. Bistability and steady-state solutions in 1D .....	3
3.1. Periodic solutions, holes, peaks and pinning.....	4
3.2. Wavenumber selection in the nonlinear regime.....	7
4. Mechanisms and pattern formation in 2D .....	8
5. Discussion .....	8
Acknowledgment.....	10
References.....	10

---

<sup>4</sup> Author to whom any correspondence should be addressed. Email: yochelis@ucla.edu

## 1. Introduction

Cardiovascular calcification, in atherosclerosis or valvular stenosis, is considered one of the most notorious cardiac diseases [1]. The initial atherosclerotic lesion is formed as a soft cellular and fibrous mass (atheroma) growing within the artery wall. A myocardial infarction (“heart attack”) occurs when the surface of the atheroma ruptures, exposing proteins that trigger clot formation in the blood. The clots then occlude the artery, preventing blood flow to the heart muscle. Little is known about the conditions under which rupture occurs. Indeed, there is even debate about whether calcium deposits mechanically stabilize or destabilize lesions [1]. Recently it was found that “*spotty*” or “*speckled*” patterns of calcification carry the greatest risk for plaque rupture, as opposed to uniform deposits [1]. Therefore, it is essential to understand the mechanism determining the patterns formed by arterial calcification.

Arterial calcification is thought to be a recapitulation of embryonic bone formation by vascular mesenchymal stem cells (VMSCs) [2], under the control of bone morphogenetic protein 2 (BMP-2) [3-5]. In *in vitro* experiments, it was shown that cultures of vascular-derived mesenchymal stem cells differentiate and indeed form calcified patterns [6]. Importantly, the morphology of the patterns was altered by applying external drugs, increasing the amount of matrix GLA protein (MGP); MGP molecules bind to active BMP-2, disabling their functionality. Thus they act as inhibitors. Assuming that the primary calcification mechanism is indeed governed by the interaction of two chemical morphogens, it is reasonable to exploit Turing’s paradigm of morphogenesis to establish the chemical pre-patterning that shape the pattern morphology.

Alan Turing, in his seminal work on morphogenesis [7], suggested that the formation of biological patterns can be understood by means of biochemistry, that is, in the reaction-diffusion framework. In this scenario, chemicals produced by cells interact as activators or inhibitors, and diffuse through the medium at distinct rates. This can create a symmetry breaking of the uniform concentrations, a mechanism that is often called a ‘diffusion-driven instability’ [8]. Since then, a number of morphogens have been identified [9] and linked to pattern development [6, 10-17]. These results suggest that an understanding of the dynamics of morphogenesis can give us a relatively simple way to understand and control biological development [16, 18-31].

The application of the Turing paradigm to biology faces the obstacle that the primary Turing instability is linear [32, 33]: the resulting pattern arises spontaneously and directly from a previously stable homogeneous condition. But the patterns we observe are presumably at large deviations from the critical conditions, and also on time scales *far* from the initial instability, i.e. cell migration is obviously much slower than chemical diffusion [34]. Consequently, even if an initial homogeneous biological system went through the Turing instability, it is impossible (using conventional methods) to experimentally demonstrate that fact.

In this article we discuss the role of low-dimensional reaction-diffusion mechanisms in promoting the mineralization patterns seen in VMSCs, as originally suggested in [6]. Using an activator-inhibitor model equation and analysis of pattern selection in the nonlinear regime, far from the any initial bifurcation, Turing or otherwise, we explain previous *in vitro* VMSC culture experiments and suggest future applications to cardiovascular calcification. The paper is organized as follows: in Section 2 we discuss a model equation that qualitatively agrees with VMSC biochemistry. Next, in Section 3 we perform a one dimensional (1D) analysis to obtain the properties of periodic and localized steady states and discuss the wave number selection in presence of multiple solutions. In Section 4, we use the latter results and secondary instabilities that operate in 2D to underline the mechanisms that lead to formation of two dimensional patterns. We conclude and discuss the medical applications in Section 5.

## 2. Activator-inhibitor model equations

The biochemical activator-inhibitor relations in a VMSC culture can be described as following. The VMSCs spontaneously express BMP-2 [35, 36] and its inhibitor-matrix GLA protein (MGP) [37, 38],

which diffuses more rapidly than the former [6]. With respect to local kinetics, it is assumed that BMP-2 obeys a saturated autocatalytic reaction [39] and directly promotes MGP production [40]. In addition, it is assumed that both substances follow a first-order degradation. In addition, BMP-2 has a chemoattractant property [36] which is responsible for cell migration following the gradients of BMP-2.

Following this description, we represent the active BMP-2 and MGP concentrations by  $a(x, y)$  and  $h(x, y)$ , respectively. The calcified patterns in VMSCs cultures, developed from a monolayer in a dish size of the order of centimeters, i.e., implying a large aspect ratio system (height vs. length) that is quasi two dimensional. In addition, since the cell migration occurs at much slower time scales than the chemical diffusion, and cells proliferate relatively slowly [41] together with the fact that neither BMP-2 nor MGP are consumed by the cells, we can neglect, to leading order, other contributions such as cell density. A qualitative activator-inhibitor model equation that of such dynamics was proposed by Gierer and Meinhardt [29, 42]

$$\begin{aligned}\frac{\partial a}{\partial t} &= D_a \nabla^2 a + \rho_a \frac{a^2 h^{-1}}{1 + q^2 a^2} - \mu_a a + A, \\ \frac{\partial h}{\partial t} &= D_h \nabla^2 h + \rho_h a^2 - \mu_h h + H,\end{aligned}\tag{1}$$

where  $\nabla^2$  is the Laplacian operator in two space dimensions,  $D_a, D_h$  are diffusion constants,  $\rho_a, \rho_h$  are cross reaction coefficients,  $\mu_a, \mu_h$  are degradation rates,  $q$  is the saturation constant, and  $A, H$  are source terms, respectively. We note that different variants and limits of this system have been discussed [20, 26, 28, 30, 31, 43].

For our application, we neglect the activator source ( $A = 0$ ), and rewrite (1) in a dimensionless form, by introducing dimensionless variables  $u = qa$ ,  $v = \mu_a qh / \rho_a$ , and scaling  $t, \mathbf{x}$  by  $\mu_a^{-1}, \sqrt{D_h / \mu_a}$ , respectively:

$$\begin{aligned}\frac{\partial u}{\partial t} &= D \nabla^2 u + \frac{u^2 v^{-1}}{1 + u^2} - u, \\ \frac{\partial v}{\partial t} &= \nabla^2 v + P u^2 - E v + S,\end{aligned}\tag{2}$$

where  $D \equiv D_a / D_h, P \equiv \rho_h / \rho_a q, E \equiv \mu_h / \mu_a, S \equiv qH / \rho_a$ . The basic model requirements to exhibit patterns are that  $D \ll 1$  and  $E > 1$  [42]. Biophysical parameter estimation from VMSC cultures [6] supports this prediction viz.  $D \sim O(10^{-2} - 10^{-3})$  and  $E > 1 \sim O(1)$ . In addition, from the same estimations,  $P \sim O(1)$ . In what follows, we consider equation (2) for the parameter values

$$D = 0.005, \quad P = 1, \quad E = 2,\tag{3}$$

with  $S$  as a *generalized* or *net* inhibition source, allowed to vary.

### 3. Bistability and steady-state solutions in 1D

Equations (2) and (3), admit three uniform solutions, one with trivial activator:

$$[u_0, v_0] = [0, S/2],\tag{4}$$

and two non-trivial

$$[u_{\pm}, v_{\pm}] = \left[ \frac{\sqrt{\theta} \pm \sqrt{\eta}}{2}, \frac{\sqrt{\theta}(\sqrt{\theta} \pm \sqrt{\eta})}{2 - (S-1)\sqrt{\theta} \pm \theta\sqrt{\eta}} \right], \quad (5)$$

where  $\eta \equiv 4/\sqrt{\theta} + \phi$ ,  $\theta \equiv \beta/3\rho + \rho/3 - 2(S+1)/3$ ,  $\phi \equiv -\theta - 2(S+1)$ ,  $\beta \equiv 1 + 14S + S^2$ ,  $\rho \equiv \sqrt[3]{\alpha/2 + \sqrt{\alpha^2/4 - \beta^3}}$ , and  $\alpha \equiv 108 - 72S(S+1) + 2(S+1)^3$ . These three uniform solutions, however, exist only for a certain range of values,  $0 < S < S_{SN}$  (see figure 1); in this range, both  $(0, v_0)$  and  $(u_+, v_+)$  are stable, defining a *bistability* region. To leading order in  $S$ ,

$$v_+ - v_0 \sim O(S^2) \quad (6)$$

and

$$u_+ - u_0 \sim 1 - \frac{S}{2} + O(S^2). \quad (7)$$

It is important to note that it is this bistability region, and in particular the large amplitude variations in the  $u$  field, that makes possible the interspersed regions of high vs. vanishing cell densities observed in VMSC cultures [6].

In bistable systems, three primary types of stationary nonuniform solutions often arise [32, 33]: (i) fronts connecting two uniform states (heteroclinic orbits in 1D physical space); (ii) periodic spatial patterns, also known as Turing patterns (limit cycles in 1D physical space); and (iii) localized states (homoclinic orbits in 1D physical space), *holes* or *peaks* superimposed on a background of a stable uniform state. The third type of state arises in systems with spatial reversibility  $[u(-x), v(-x)] \rightarrow [u(x), v(x)]$  [44]. In the following, we discuss the implications of periodic (ii) and localized (iii) solutions, while solutions of type (i) are discussed in [45].

### 3.1. Periodic solutions, holes, peaks and pinning

The Turing instability of the  $(u_+, v_+)$  state [46], gives rise to subcritical bifurcations of periodic and localized hole solutions. We compute the branches of these steady states by setting  $\partial_t u = \partial_t v = 0$  in (2), and using a numerical continuation method [47]. The results are represented in terms of

$$N = \sqrt{L^{-1} \int_0^L \left\{ u^2 + v^2 + (\partial_x u)^2 + (\partial_x v)^2 \right\} dx} \quad (8)$$

where  $L$  is the spatial period; temporal stability is determined by a numerical eigenvalue method. The bifurcation diagram of 1D steady state solutions of (2), is represented in figure 1.

The periodic state  $L = L_T$ , and the hole states  $L = H_{0,\pi}$  appear as unstable small amplitude solutions around the  $(u_+, v_+)$  solution (see profile (a) in figure 1) and become large amplitude, with respect to the activator, at the first saddle node (see profile (b), (e), (f) in figure 1). The odd and even hole branches form a pinning region. In variational systems, these oscillations cause an effective broadening of

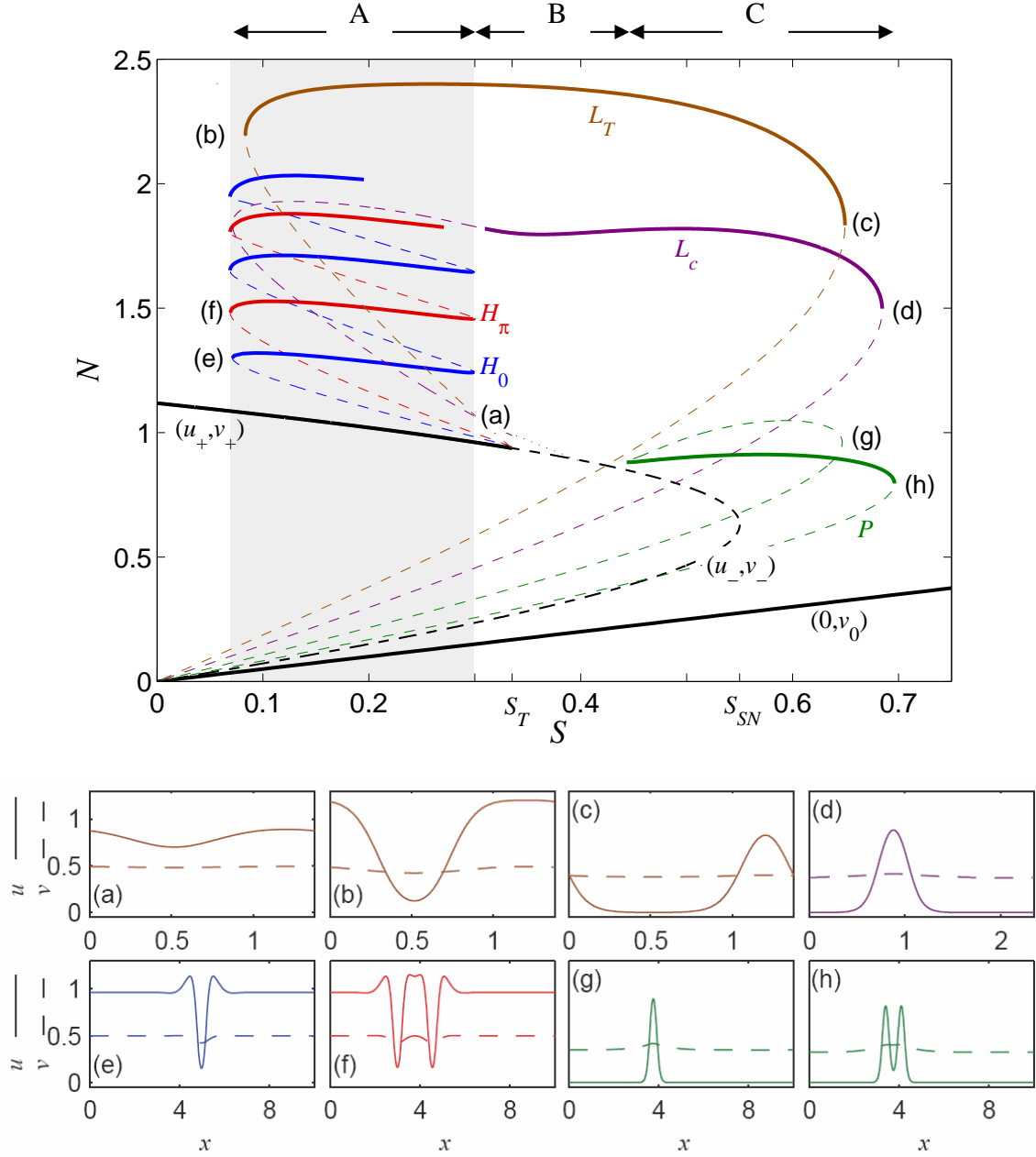


**Figure 1.** Top panel: Bifurcation diagram showing branches of uniform solutions,  $(0, v_0), (u_+, v_+)$ , periodic solutions,  $L = L_T$ , (a-c),  $L = L_c$ , (d), localized holes with even number  $H_0$ , (e), with odd number  $H_\pi$ , (f), and localized peaks  $P$ , (g,h), as a function of  $S$ . Solid lines mark stable portions of the branch; the shaded region represents the pinning regime of the isolated hole state (e) and bounded multiple-hole solutions such as (f). (a-h) are  $u$  and  $v$  profiles computed at locations indicated in the upper panel. Period length:  $L_T \equiv 2\pi/k_T \approx 1.38, L_c \approx 2.34, H_{0,\pi} = P = 10$ , where  $k_T$  is the Turing mode obtained at  $S = S_T$ . We verified that (e-f) are indeed localized solutions by increasing the period to  $L = H_{0,\pi} = P = 100$ .

the Maxwell point [48-52] at which a heteroclinic orbit (Pomeau front) between the uniform and periodic solutions is time independent [53], see the shaded region in figure 1.

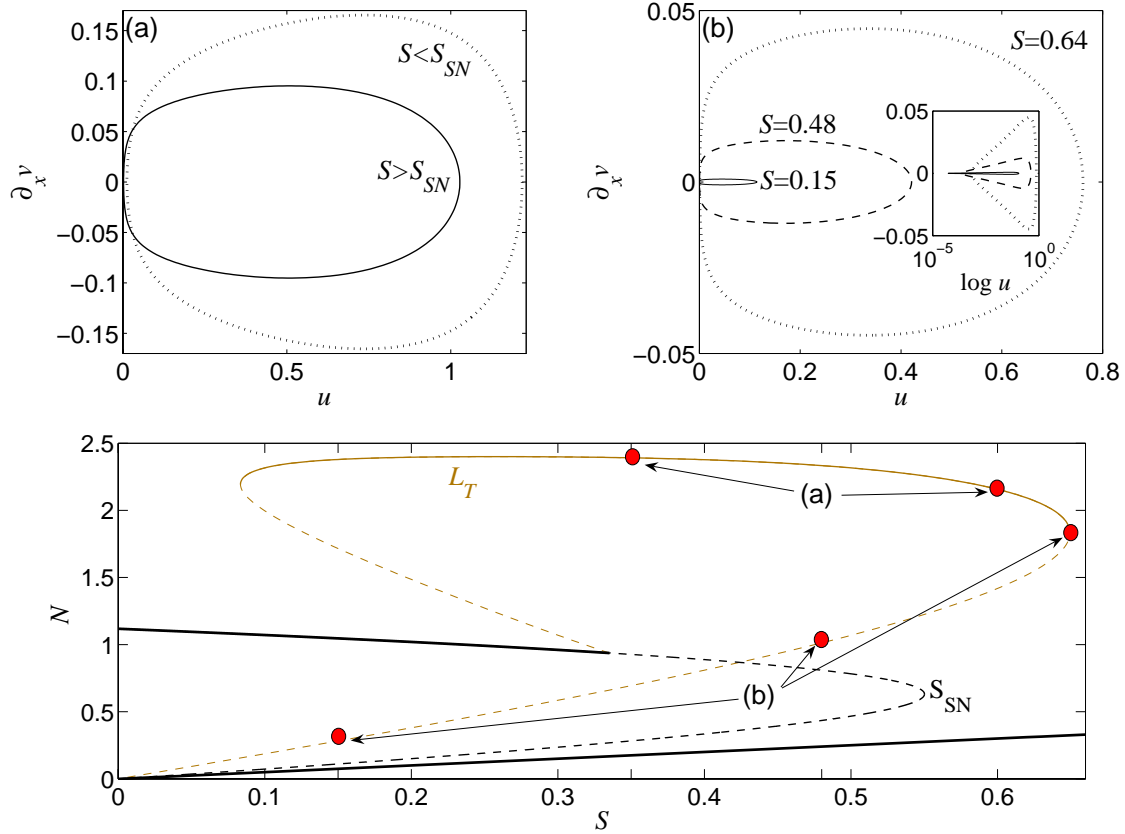


**Figure 2.** Trajectory of the periodic Turing solution in a phase portrait  $u$  vs.  $\partial_x v$ , along (a) stable and (b) unstable branches as depicted in the bottom panel. The inset in (b) shows the half plane as a function of  $\log u$ , to emphasize the trajectory approach towards the fixed point  $(u, v) = (0, v_0)$  as  $S \rightarrow 0$ .

As  $S$  is increased above  $S_T$ , the  $(u_+, v_+)$  solution becomes unstable to additional wavenumbers, which also bifurcate subcritically. For simplicity, we have shown only the solution with the longest period,  $L = L_c$ . Surprisingly, as can be seen in figure 1, all the periodic solution branches terminate at the onset of the transcritical bifurcation,  $S = 0$ . In addition, by prolongation of the periodic solutions' period in the vicinity of  $S = 0$ , one can compute also the localized states that exponentially asymptote to  $(0, v_0)$ , see profiles (g,h) in figure 1. However, unlike the possible multiplicity of stable bounded hole solutions, only a single peak can stabilize (see profile (h) in figure 1) while the double peak solution (see profile (g) in figure 1) is unstable, implying a *repulsive* interaction between two neighboring peaks.

To understand this nontrivial behavior we exploit a phase space representation [44, 51],  $u$  vs.  $\partial_x v$ . The Turing instability of the  $(u_+, v_+)$  state corresponds to a reversible Hopf bifurcation in space [44], that is a stable periodic Turing state,  $L = L_T$ , that is, a limit cycle. The limit cycle persists above  $S = S_{SN}$  (see figure 2a), however it approaches the  $(0, v_0)$  state and finally, after the right saddle node (see figure 1), vanishes as  $S \rightarrow 0$  (see figures 1 and 2b). This forms an effective Pomeau front at  $S = 0$ . The peak states asymptote to  $(0, v_0)$  at  $x \rightarrow \pm\infty$  as

$$\begin{pmatrix} u \\ v \end{pmatrix} - \begin{pmatrix} 0 \\ v_0 \end{pmatrix} \propto e^{\lambda x}, \quad (9)$$

where the four eigenvalues are real,  $\lambda = \pm\sqrt{E} = \pm\sqrt{2}$  and  $\lambda = \pm\sqrt{1/D} = \pm\sqrt{200}$ , and are associated with two stable  $W^S[(0, v_0)]$  and two unstable  $W^U[(0, v_0)]$  manifolds [44]. By symmetry,  $W^S[(0, v_0)] = -W^U[(0, v_0)]$  with respect to the  $\partial_x u = \partial_x v = 0$  plane. Since all states collapse with a vanishing amplitude at the transcritical bifurcation onset,  $S = 0$ , the stable and unstable manifolds of the effective Pomeau front coalesce with the stable and unstable manifolds of homoclinic  $P$  states. Pinning in the direction  $S > 0$  is impossible, due to repulsive interactions between  $P$  states, see figure 1.

### 3.2. Wavenumber selection in the nonlinear regime

Near the bifurcation onset, here Turing, wavenumber selection or *mode interaction* can be addressed using a weakly nonlinear analysis [32, 54]. However, in our case all bifurcations are subcritical and the solutions stabilize *far* from the Turing onset, i.e., the weakly nonlinear analysis is not applicable. On the other hand, the nonlinear regime exhibits coexistence of multiple stable solutions, making it hard to foresee the wavenumber selection and the sensitivity to initial conditions; both determine the basin of attraction of the final states. To simplify the analysis, we focus here on three regions distinguished by coexisting solutions (see figure 1): (A) holes and periodic states; (B) periodic states with periods  $L_T \leq L \leq L_c$ ; and (C) periodic and isolated states (that is, localized peaks with  $L \geq L_T$ ).

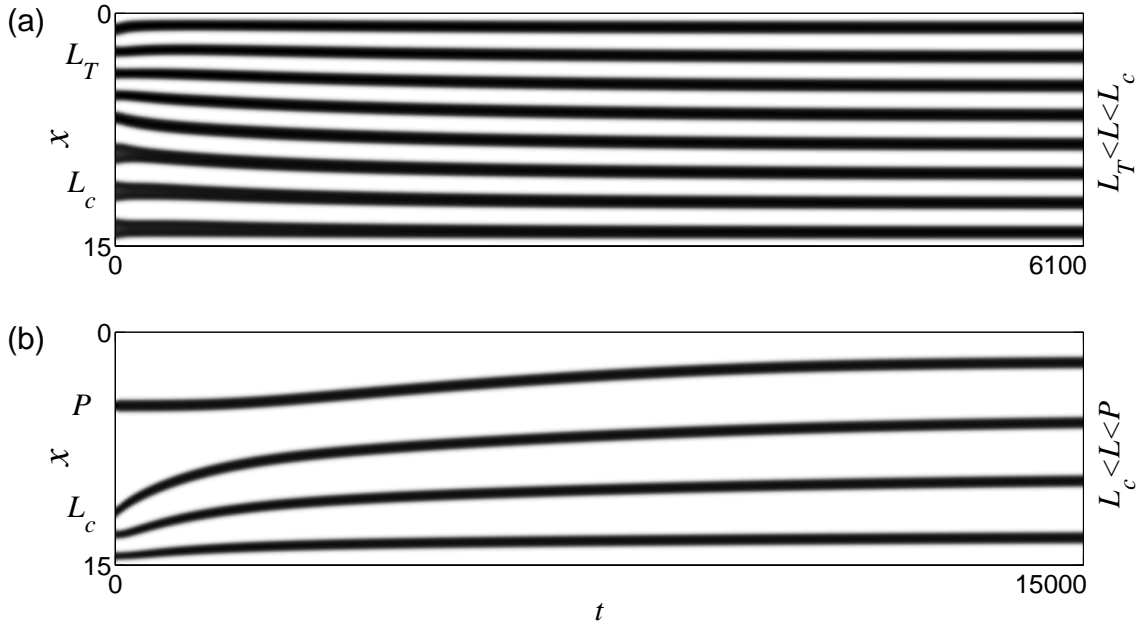


**Figure 3.** Space-time plots showing the temporal evolution of an initial condition that is a combination of (a)  $L_T \approx 1.38$  and  $L_c \approx 2.34$ , and (b)  $L_c$  and  $P$  (as indicated at  $t = 0$ ). Equation (2) was integrated in 1D with Neumann boundary conditions; a grey-scale map shows the  $u$  field. Parameters: (a)  $S = 0.35$ , (b)  $S = 0.5$ .

Since in the pinning region (A), fronts between localized and periodic solutions are stationary, we refer the reader to [49], and discuss in the following only regions (B) and (C). In both regions, a spatially nonuniform initial condition that, for example, features two different length scales in two parts of the domain, results in *mode compromise*: the asymptotic periodicity is a compromise value between two initial states, implying dispersion of the front separating two domains with different periodicities rather than invasion, see figure 4. When we initiated a domain with two different stable solutions coexisting in regions (B) and (C), it then evolved into a single final pattern, whose length scales were intermediate, which are also stable solutions of (2) (Figs. 3a and 3b, respectively).

#### 4. Mechanisms and pattern formation in 2D

It is well-known that reaction diffusion systems can exhibit transverse and curvature-induced instabilities in 2D [32, 33], so that labyrinthine or spotted patterns can form respectively, through secondary zigzag or varicose instabilities of stripes [55] or through an instability of axisymmetric spots [56]. Thus, we have performed an extended numerical investigation to obtain the formation mechanisms of the diverse patterns; the results are described in detail in figure 4.

First, we have numerically calculated the regions of curvature, zigzag, and varicose instabilities of *all* solutions: periodic, isolated stripes, isolated and bounded localized spots; the results are indicated as instability types in figure 4. To demonstrate the effect of these instabilities on the asymptotic pattern, we have integrated equation (2) in 2D just above the Turing onset, starting from infinitesimal random perturbations around the uniform  $(u_+, v_+)$  state; as expected due to the zigzag instability, a labyrinthine pattern was formed (see inset (a) in figure 4).

Next, we used this pattern as an initial state for other values of  $S$ , the results are shown in insets (b-g). The domain of labyrinthine patterns ranges from the bistability onset at  $S = S_{SN}$  (inset (b) in figure 4) to the 2D pinning region (inset (c) in figure 4), however only for  $S_T < S < S_{SN}$  do they form spontaneously, due to the Turing instability of the uniform  $(u_+, v_+)$  state. In a small region above  $S_{SN}$ , single peak spots are unstable, so that straight stripe fragments may form; this leads to the formation of periodic states consisting of both spots and stripe fragments (inset (d) in figure 4). As a single spot stabilizes, the pattern becomes ultimately spotted. However, according to figure 1, the pattern may admit distinct periodicities under other initial conditions; numerical 2D computations support this prediction, as insets (e-f) in figure 4 show. We note that both states (e-f) are not asymptotic and approach asymptotically to a hexagonal symmetry, however, since the interaction between localized states is weak, this process is very slow, as can be observed from the repulsive motion of three initially close localized peaks (inset (j) in figure 4). For small  $S$  values (that is, in the 2D pinning region), we obtain an image inverse to peak spots, that is, distributed *hole spots* (inset (g) in figure 4). In the absence of repulsive interactions between neighboring holes, see insets (h-i) in figure 4, the hole spots support coexisting clusters, as shown in inset (g).

#### 5. Discussion

In this paper, we theoretically studied the mechanisms of pattern formation that give rise to many steady state patterns in a well known activator-inhibitor model [29, 42]. We chose a bistable version, obtained by keeping the inhibition source term, and employing a saturated autocatalytic local kinetics. This qualitative form, and the values of the other parameters, were made to keep fidelity with our main application, which is the formation of calcified patterns by vascular mesenchymal stem cells (VMSCs) [6]. These are the cells that are thought to form bone in atherosclerotic plaque, the primary process that has been linked to atherosclerotic calcification [2]. For simplification, we have excluded from this model any higher order contributions, such as the contributions of changing cell densities. While cell density is expected to have a minor role in the initial qualitative pattern selection, it may quantitatively modify the pattern architecture



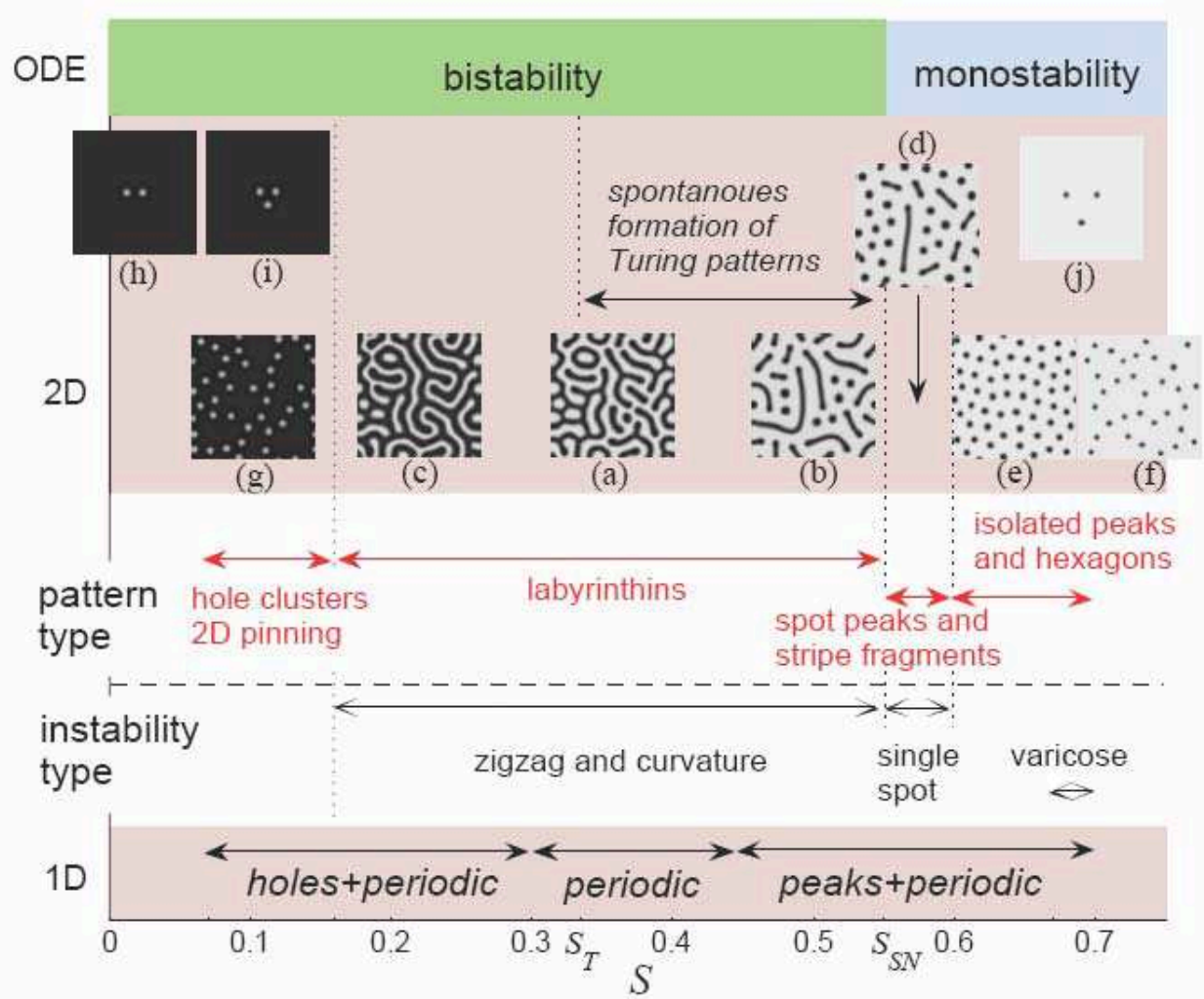


**Figure 4.** Diagram showing the instabilities and the corresponding patterns forms as a function of  $S$ . The two dimensional patterns were obtained via numerical integration of (2) with periodic boundary conditions on a  $x = y = [0, 15]$  physical domain; a grey-scale map shows the  $u$  field. Labyrinthine patterns (a) were generated from infinitesimal random perturbations around  $(u_+, v_+)$ , and used as initial conditions for (b-g). The spotted patterns (e-g) are not asymptotic; they are shown for  $t = 3000$ . The repulsive interactions between the peak spots in (e-f) are very weak, however the final state eventually approaches hexagonal symmetry, while in (g) there is deformation towards hole clusters rather than to hexagonal symmetry. Localized patterns (h-i) are examples of the pinning phenomenon that persist in two dimensions. Pattern (j) was generated from an inverse image of (i), but due to the repulsive interactions the three peaks move away from each other. Parameters: (a)  $S = 0.35$ , (b)  $S = 0.53$ , (c)  $S = 0.2$ , (d)  $S = 0.58$ , (e)  $S = 0.62$ , (f)  $S = 0.69$ , (g-i)  $S = 0.1$ , (j)  $S = 0.69$ .

at later time stages. The extension of the Gierer-Meinhardt model to include the contributions of cell density is beyond the scope of this paper, and will be discussed elsewhere.

While different forms of the Gierer-Meinhardt model have been studied, and a number of interesting qualitative phenomena have been found [20, 26, 28, 30, 43], we present here a generalized and detailed view of the multiple periodic and localized states that occur in this model, as well as their basins of attraction. Our method, therefore, is part of a full nonlinear analysis, far from the onset of the Turing instability. In particular, we show that the majority of patterns form subcritically, that is, by “large”

amplitude perturbations, as shown in figures 1 and 4. First, we exploited the powerful tool of spatial dynamics, incorporated with temporal stability, to identify the primary instabilities. Then we unfolded the possible stable and unstable 1D solution branches as a function of the inhibition source,  $S$  (see figure 1). We used this analysis to calculate in detail the secondary instabilities and the parameter regions in which 2D patterns, such as labyrinths, mixtures of spots and stripe fragments, and bounded vs. isolated spots, can form (see figure 4).

Importantly, a spontaneous formation of labyrinthine and spotted patterns (with roughly hexagonal symmetry) have been indeed observed in *in vitro* experiments in VMSC preparations [6]. In these experiments the inhibition source was altered by external addition of MGP, the inhibitor of the activator BMP-2. As in our analysis, labyrinthine patterns have been found at lower concentrations of added MGP (corresponding to lower  $S$  values) while at higher MGP concentrations (corresponding to higher  $S$  values) roughly periodic spotted patterns were developed. Moreover, in other experiments, at even higher inhibitor values, (that is, higher than the basin of attraction of periodic patterns), isolated localized spots are formed, as also predicted by our analysis [46].

The good qualitative agreement between the theoretical analysis and the experimental observations suggests a novel strategy for the biochemical control of calcified patterns, via the framework of morphogenesis. There are several potential applications of this strategy. First, as noted above, the spotted patterns of calcification seen in culture dishes are considered a good model for the formation of spotty atherosclerotic calcification in humans [1]. If these calcified deposits become confluent, it has been conjectured that the resulting solid mass is expected to mechanically stabilize the adjacent lesion, while if the calcification remains ‘spotty’, there is an increased risk of rupture and myocardial infarction [1].

A second application is to the formation of bone tissue (by the same types of cells). Trabecular bone has a dense labyrinthine and hole architecture, presumably formed by the same morphogenetic processes, so our analysis may also be relevant to bone regeneration.

## Acknowledgment

We thank Edgar Knobloch, John Burke and Kristina Boström for helpful discussions.

## References

- [1] Abedin M, Tintut Y and Demer L L 2004 *Arterioscler Thromb Vasc Biol* **24** 1161-70
- [2] Abedin M, Tintut Y and Demer L L 2004 *Circ Res* **95** 671-6
- [3] Tintut Y, *et al.* 2003 *Circulation* **108** 2505-10
- [4] Hruska K A, Mathew S and Saab G 2005 *Circulation Research* **97** 105-14
- [5] Shao J S, Cai J and Towler D A 2006 *Arterioscler Thromb Vasc Biol* **26** 1423-30
- [6] Garfinkel A, *et al.* 2004 *Proc Natl Acad Sci* **101** 9247-50
- [7] Turing A M 1952 *Philos Trans R Soc London, Ser B* **237** 37-72
- [8] Maini P K, Painter K J and Chau H N P 1997 *Journal of the Chemical Society-Faraday Transactions* **93** 3601-10
- [9] Lander A D 2007 *Cell* **128** 245-56
- [10] Sick S, Reinker S, Timmer J and Schlake T 2006 *Science* **314** 1447-50
- [11] Morris H R, *et al.* 1987 *Nature* **328** 811-4
- [12] Chen Y and Schier A F 2001 *Nature* **411** 607-10
- [13] Harris M P, *et al.* 2005 *Proc Natl Acad Sci* **102** 11734-9
- [14] Painter K J, Maini P K and Othmer H G 1999 *Proc Natl Acad Sci* **96** 5549-54
- [15] Yamaguchi M, Yoshimoto E and Kondo S 2007 *Proc Natl Acad Sci* **104** 4790-3
- [16] Liu R T, Liaw S S and Maini P K 2006 *Phys Rev E Stat Nonlin Soft Matter Phys* **74** 011914
- [17] Yu M, Wu P, Widelitz R B and Chuong C M 2002 *Nature* **420** 308-12

- [18] Hunding A and Sorensen P G 1988 *J Math Biol* **26** 27-39
- [19] Murray J D and Oster G F 1984 *IMA J Math Appl Med Biol* **1** 51-75
- [20] Arcuri P and Murray J D 1986 *J Math Biol* **24** 141-65
- [21] Dillon R, Maini P K and Othmer H G 1994 *J Math Biol* **32** 345-93
- [22] Klein C T 1998 *J Theor Biol* **194** 263-74
- [23] Crampin E J, Gaffney E A and Maini P K 1999 *Bull Math Biol* **61** 1092-120
- [24] Barrio R A, Varea C, Aragon J L and Maini P K 1999 *Bull Math Biol* **61** 483-505
- [25] Hunding A 1987 *J Math Biol* **25** 109-21
- [26] Ward M J, *et al.* 2002 *SIAM J Appl Math* **62** 1297-328
- [27] Mimura M A and Nishiura Y 1979 *J Math Biol* **7** 243-63
- [28] Kolokolnikov T, Sun W, Ward M and Wei J 2006 *SIAM J Appl Dyn Syst* **5** 313-63
- [29] Gierer A and Meinhardt H 1972 *Kybernetik* **12** 30-9
- [30] Murray J D 2002 *Mathematical Biology* (New York: Springer)
- [31] Hillen T 2007 *SIAM Rev* **49** 35-51
- [32] Cross M C and Hohenberg P C 1993 *Rev Mod Phys* **65** 851-1112
- [33] Pismen L M 2006 *Patterns and Interfaces in Dissipative Dynamics* (Berlin Heidelberg: Springer-Varlag)
- [34] Page K M, Monk N A M and Maini P K 2007 *Phys Rev E* **76** 011902 (1-15)
- [35] Boström K, *et al.* 1993 *Journal of Clinical Investigation* **91** 1800-9
- [36] Willette R N, *et al.* 1999 *J Vas Res* **36** 120-5
- [37] Boström K, *et al.* 2001 *J Biol Chem* **276** 14044-52
- [38] Zebboudj A F, Imura M and Boström K 2002 *Journal of Biological Chemistry* **277** 4388-94
- [39] Ghosh-Choudhury N, *et al.* 2001 *Biochem Biophys Res Commun* **286** 101-8
- [40] Zebboudj A F, Shin V and Boström K 2003 *J Cell Biochem* **90** 756-65
- [41] Bennett R L, Navab M, Demer L L and Fogelman A M 1993 *Arterioscler Thromb* **13** 360-6
- [42] Koch A J and Meinhardt H 1994 *Rev Mod Phys* **66** 1481-507
- [43] Doelman A and van der Ploeg H 2002 *SIAM J Appl Dyn Syst* **1** 65-104
- [44] Champneys A R 1998 *Physica D* **112** 158-86
- [45] Yochelis A and Garfinkel A unpublished
- [46] Yochelis A, *et al.* unpublished
- [47] E. Doedel *et al.* AUTO2000: Continuation and bifurcation software for ordinary differential equations: Technical report, Concordia University; 2002.
- [48] Woods P D and Champneys A R 1999 **129** 147-70
- [49] Burke J and Knobloch E 2006 *Phys Rev E* **73** 056211
- [50] Burke J and Knobloch E 2007 *Phys Lett A* **360** 681-8
- [51] Gomila D, Scroggie A J and Firth W J 2007 *Physica D* **227** 70-7
- [52] Couillet P 2002 *Int J Bifurcation Chaos* **12** 2445-57
- [53] Pomeau Y 1986 *Physica D* **23** 3-11
- [54] Hoyle R B 2006 *Pattern Formation: An Introduction to Methods* (Cambridge: University Press)
- [55] Hirschberg P and Knobloch E 1993 *Chaos* **3** 713-21
- [56] Kolokolnikov T and Tlidi M 2007 *Phys Rev Lett* **98** 188303